Journal of Science and Transport Technology
Journal homepage: https://jstt.vn/index.php/en

GIS-Based Flow-R Model for Debris Flow Susceptibility Mapping: A Case Study from Muong Bo, Lao Cai, Vietnam

Nguyen Cong Dinh[1], Nguyen Duc Manh[1*], Nguyen Chau Lan[1], Nguyen Anh Tuan[1], Indra Prakash[2], Vu Quang Dung[3], Nguyen Trung Kien[4], Do Tuan Nghia[5], Nguyen Van Thang[5]

[1]University of Transport and Communications, Hanoi 100000, Vietnam
[2]DDG (R) Geological Survey of India, Gandhinagar 382010, India
[3]Geotechnical and Artificial Intelligence research group, University of Transport Technology, Hanoi 100000, Vietnam
[4]Institute of Earth Sciences - Vietnam Academy of Science and Technology, Hanoi, Vietnam
[5]Department of Civil Engineering, Thuyloi University, Hanoi, Vietnam

Article info
Type of article:
Original research paper

DOI:
https://doi.org/10.58845/jstt.utt.2026.en.6.1.29-47

***Corresponding author:**
Email address:
nguyenducmanh@utc.edu.vn

Received: 10/10/2025
Received in Revised Form: 20/11/2025
Accepted: 04/12/2025

Abstract: Landslides and debris flows are frequent hazards in Vietnam's mountainous regions, causing severe socio-economic damage that has intensified under climate change and extreme rainfall conditions. This study applies the open-source GIS-based Flow-R model to assess debris-flow susceptibility and runout characteristics in Muong Bo Commune, Lao Cai Province, northwestern Vietnam (specifically focusing on the highly vulnerable area around the Nam Cang stream). The methodology involved developing a geospatial database and simulating potential initiation and propagation zones. A major debris-flow event that occurred on 12 September 2023 was used for model calibration and validation. Field validation confirmed the model's robust capability to simulate flow runout distances based on observed data. Seventy percent of the mapped debris-flow initiation points were used for calibration, and 30% for validation[/RED], and model performance was evaluated using the Area Under the ROC Curve (AUC). The Flow-R model achieved an AUC value of 0.868, indicating good predictive capability[/RED], while 48.5% of observed debris-flow initiation points were correctly predicted. Results demonstrate that Flow-R effectively delineates high-susceptibility source zones and plausible debris-flow runout paths, particularly for medium- to large-scale events. The novelty of this study lies in the first integrated application of Flow-R, combined with systematic field validation in northwestern Vietnam, and the coupling of detailed geological–geomorphological characterization with susceptibility and runout modeling, providing a transferable framework for debris-flow assessment in data-scarce mountainous regions.

Keywords: Landslide, Debris flow, Flow-R, Susceptibility mapping, Runout modelling, Remote sensing.

1. Introduction

Vietnam's northern mountainous provinces, including Son La, Lai Chau, Dien Bien, Yen Bai, and Lao Cai, are among the most landslide- and

debris-flow-prone regions in Vietnam [1–3]. The combination of steep topography, intense monsoonal rainfall, complex geology, and active geomorphological processes makes these areas particularly vulnerable to rainfall-induced slope failures. In recent decades, the frequency and intensity of such hazards have increased due to climate change, extreme precipitation events, and anthropogenic disturbances, including deforestation, road construction, and slope modification [4–6].

Debris flows are rapid, gravity-driven mixtures of water, soil, rock fragments, and organic material that typically initiate from shallow landslides on steep slopes and subsequently mobilize within channels [7, 8]. While the term landslide broadly encompasses all types of mass movement, in the context of debris flow, landslides typically refer to the initial slope failures (slides or slumps) that occur on steep slopes. Unlike deep-seated landslides, debris flows are characterized by high mobility, long runout distances, and sudden onset, which significantly increases their destructive potential. In the mountainous regions of northwestern Vietnam, shallow landslides frequently act as source areas that transform into debris flows during intense rainfall, underscoring the need to distinguish clearly between initiation processes and flow propagation mechanisms.

Recent advances in remote sensing and geographic information systems (GIS) have enabled more systematic assessment of landslide and debris-flow susceptibility through the integration of topographic, geological, hydrological, and land-cover data [9–13]. Among GIS-based approaches, the Flow-path assessment of gravitational hazards at a Regional scale (Flow-R) model has been widely applied for simulating debris-flow initiation and runout at regional to local scales [14–17]. Flow-R is particularly well-suited for mountainous regions where detailed geotechnical and hydrological data are limited, as it relies primarily on topographic and geomorphological controls.

In Vietnam, however, most previous studies have focused on regional susceptibility mapping, with limited attention to debris-flow propagation, and very few studies have integrated field-based validation of real events [3, 4, 18]. Although Flow-R has been successfully applied internationally, its application in Vietnam remains rare and largely unvalidated, particularly in the context of observed debris-flow events, representing a clear knowledge gap.

The objective of this study is therefore to apply and validate the Flow-R model for debris-flow susceptibility and runout assessment in Muong Bo Commune, Lao Cai Province, using the well-documented Nam Cang debris-flow event of 12 September 2023. Specifically, the study aims to (i) develop a comprehensive geospatial database integrating remote sensing and field data, (ii) simulate debris-flow initiation and propagation zones using Flow-R, and (iii) evaluate model performance through quantitative validation metrics. By explicitly addressing model assumptions and limitations, this work contributes a scientifically robust and operationally useful framework for debris-flow assessment in data-scarce mountainous regions of Vietnam and similar settings worldwide. The outcomes provide scientifically grounded and spatially explicit hazard maps, offering essential inputs for natural hazard mitigation, land-use regulation, and sustainable development planning under the growing influence of climate change.

2. Study area and material

2.1. Geography, topography, and climate

Muong Bo Commune is located in the South-Southeast, approximately 50 km from Lao Cai City (Fig. 1), characterized by diverse and complex topography. Altitudes range from 140m to 3150m, with slopes varying from 0 to 80 degrees. The terrain is divided into distinct areas by streams, forming a basin tilted towards the Northeast, Northwest, and Southeast (Fig. 1). The focus of this study is primarily on the Nam Cang stream area, which represents a highly vulnerable sub-region

within the commune, although the boundaries of the whole commune are used for regional analysis. The characteristics of slope class distribution in the study area are detailed in Table 1.

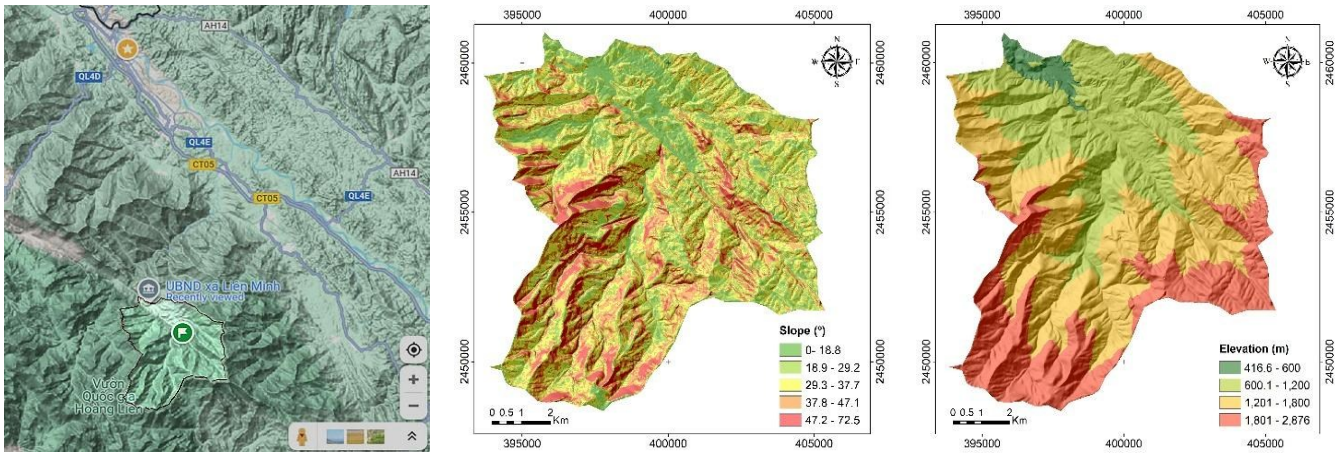

Fig. 1. Location of the study area in Muong Bo Commune (left), map of slope distribution (middle), and map of terrain elevation class distribution (right)

Table 1. Characteristics of slope class and terrain elevation distribution in the study area

Terrain Slope (degrees)	Area Percentage (%)	Terrain Elevation Class	Elevation Range (m)	Area Percentage (%)
0-16	7.69	Class II	416.6-600	2.53
17-25	14.22	Class III	600.1-1200	28.38
25-35	32.85	Class IV	1200.1-1800	39.76
35-45	31.96	Class V	1800.1- 2876	26.43
45-80	13.29			
Total	100	Total		100

The study area is located within the geological structure of the Red River Shear Zone and the Fansipan Zone. The commune is divided into four terrain elevation classes (II-V), which are detailed in Fig. 1. Table 1 provides information on the area and percentage distribution of each terrain elevation class. The study area has a humid subtropical climate, characterized by a rainy season that can experience extreme heavy rainfall or prolonged periods of rain, resulting in significant water accumulation.

The area has a dense network of rivers and streams, with varying densities (Fig. 2). The dominant land cover is evergreen forest (82.072%), with other types including residential areas, rice fields, and planted forests (Fig. 2). Detailed statistics on land cover characteristics of the study area are presented in Fig. 3.

The region experiences a humid subtropical monsoon climate, with average annual rainfall ranging from approximately 1,800 to 2,500 mm, of which more than 70% occurs during the May–September rainy season. Extreme short-duration rainfall events, often exceeding 81.2 mm in one hour, are common during intense convective storms and typhoons, and are recognized as primary triggers for debris flows in the area. Prolonged antecedent rainfall frequently leads to near-saturated soil conditions, further reducing slope stability.

2.2. Stratigraphy, geological structure, and tectonic activity

The geological structure of the study area is complex and strongly influenced by regional tectonics, characterized by multiple fault systems and diverse lithological units (Fig. 4; [19]). The study site is situated at the end of a straight valley that extends in a Northwest-Southeast direction,

following one of the primary faults within the dominant fault system in the area, which has a Northwest-Southeast orientation [20]. This fault system, combined with secondary perpendicular faults, creates compressed and fractured zones due to tectonic geological activities. The surrounding highlands are composed mainly of the Ye Yen Sun Complex ($\gamma\xi K–\rho ys_{1-2}$, $\rho\gamma K–\rho ys_3$), intruded locally by rocks of the Po Sen Complex (ρPZ_1ps_2, $\delta\gamma PZ_1ps_1$) and underlain by the Sinh Quyen Formation ($PR_{1-2}sq$).

The lithological units generally exhibit massive structures with poor bedding or lamination, limiting the occurrence of planar or wedge-type failures along distinct structural planes. The slopes of the hills in the study area are composed of loose materials, typically weathered layers of the contact zones between the Po Sen and Ye Yen Sun intrusive bodies. However, the presence of fractured and weathered zones, combined with water saturation in fine-grained layers, significantly enhances the potential for gravitational sliding and debris flow initiation during intense rainfall events. The tectonic activity associated with regional fault systems continues to influence local geomorphology and slope stability, maintaining a dynamic and evolving geological environment.

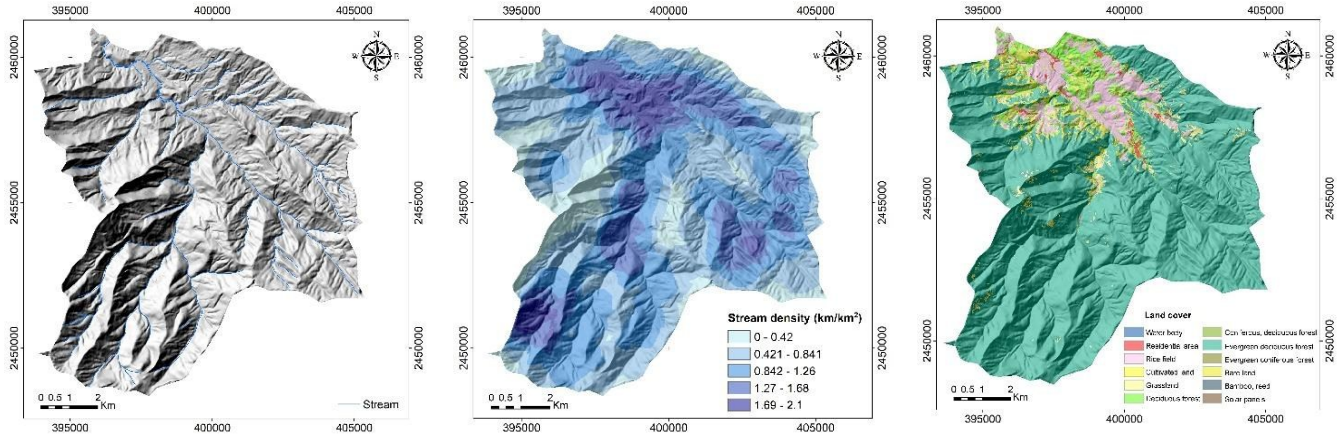

Fig. 2. Map of stream distribution (left), stream density (middle), and land cover distribution (right) in the study area (based on Sentinel-2 image processing results in 2020)

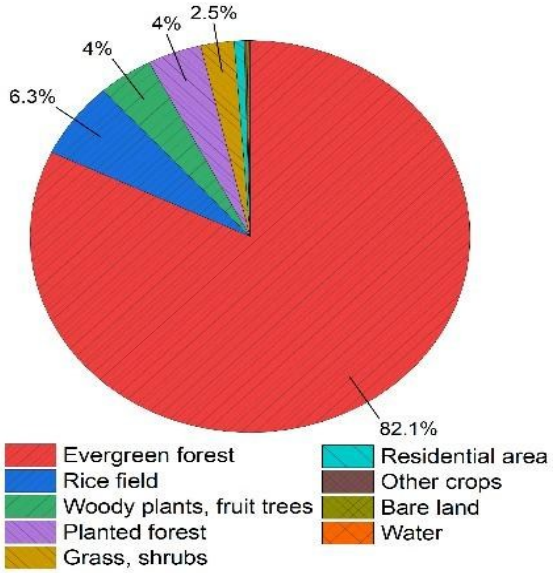

Fig. 3. Statistics of land cover characteristics in the study area

2.3. Preliminary Investigation of Nam Cang Debris Flow (September 12, 2023)

On September 12, 2023, a debris flow occurred in Muong Bo Commune, Lao Cai,

resulting in significant impacts in the area, particularly within the Nam Cang stream watershed. The area affected by the debris flow has a total basin area of approximately 1,759 ha, including seven stream branches. The distances from the Topas Riverside Lodge (TRL) area to the affected locations N1 and N2 were approximately 88m and 245m, respectively. According to local observations, the water level in the stream began to rise around 7:30 PM on September 12. By 8:30 PM, the floodwaters had risen higher and peaked around 8:40 PM, even submerging the second floor of a large house belonging to Topas Riverside. The debris flow occurred between 8:30 PM and 8:40 PM, carrying away many large trees and hundreds of large boulders (estimated 1-2 tons) [21].

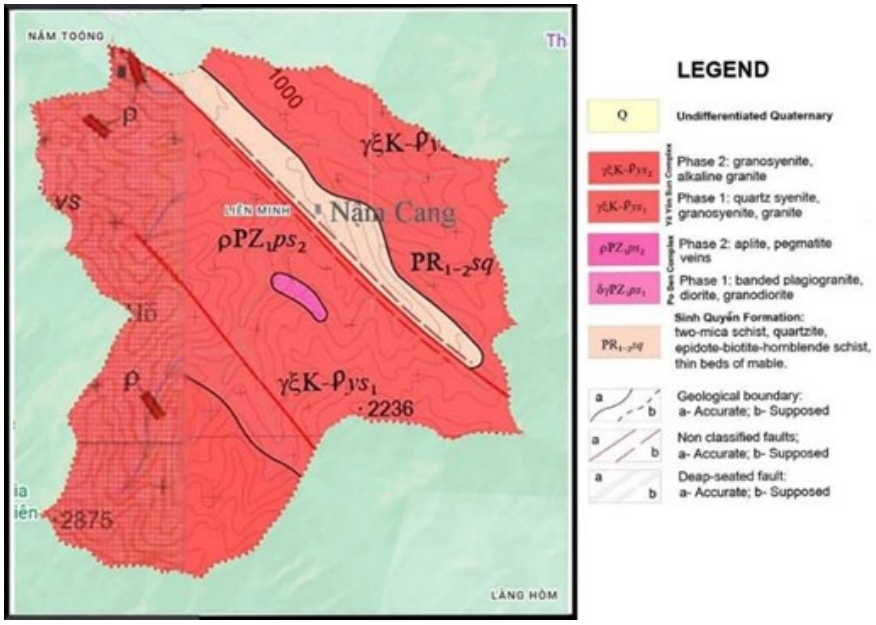

Fig. 4. Stratigraphy and geological structure map of the Nam Cang area (Muong Bo Commune, Lao Cai, Vietnam), reproduced from Tran Xuyen et al. (2000).

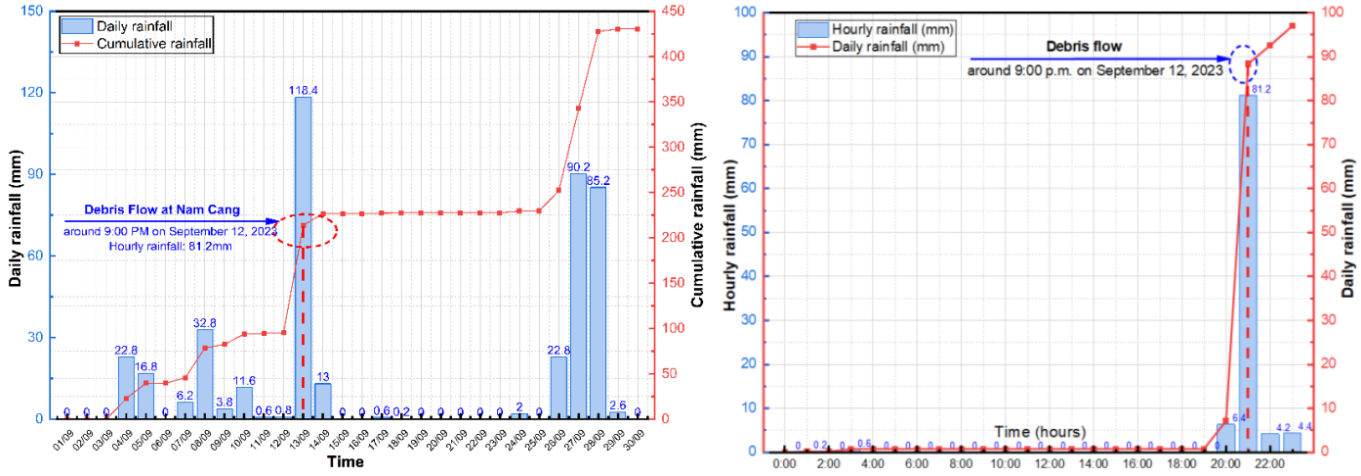

Fig. 5. Hourly and daily rainfall distribution recorded at the Ta Thang Hydropower Station on September 12, 2023

Rainfall data near the Topas Riverside area showed nine consecutive days of light rain preceding the event, followed by hefty rainfall that lasted approximately 1 hour. Specifically, rainfall in 1 hour reached up to 81,2 mm in some places (at Ta Thang, Fig. 5). This rainfall in a short period is considered the main factor causing the debris flow. Additionally, large trees and boulders carried by the flow caused stream blockages at two locations, approximately 200 meters and 250 meters

upstream from Topas Riverside (Fig. 6). When the water volume was sufficient, these two blockage points broke, causing a large debris flow to flow down to the downstream area (Fig. 7).

Fig. 6. Debris flow analysis diagram at Nam Cang on September 12, 2023

Fig. 7. Accumulated rock and debris flow in the stream (Topas Riverside)

3. Methodology

3.1. Fields investigation

The field investigation of the debris-flow area in Nam Cang was conducted in two campaigns: on October 22–23, 2023, following the debris-flow event, for field surveying, measurement, and evaluation; and on November 6, 2023. The field methods implemented included topographic surveys using an uncrewed aerial vehicle (UAV) and sampling at the debris flow locations.

3.2. Geotechnical testing methods

Soil and rock samples were collected, and laboratory tests were conducted at Thuyloi University. Geotechnical tests were performed using six soil samples and two rock samples (M1 and M2). For soil samples, the particle size distribution was determined according to ASTM D422. The Liquid limit and Plastic limit were determined in accordance with ASTM D 4318. Following physical tests, several mechanical tests were conducted, including direct shear tests and permeability tests, in accordance with the ASTM D698 and ASTM D3080 standards, respectively. For rock samples, axial compressive tests were conducted under both dry and saturated conditions, in accordance with ASTM D1143.

3.3. Numerical simulation using Flow-R

To evaluate debris flow susceptibility in Muong Bo Commune, the Flow-R model was applied within a GIS framework using spatial, geological, and geomorphological datasets. The methodology integrates remote sensing data, field observations, and numerical simulation to delineate potential initiation and propagation zones

of debris flows. The overall workflow involves setting up the model, preparing the data, selecting the algorithm, and validating the simulation outputs.

3.3.1. Flow-R Model

The Flow-R model is a two-dimensional surface flow propagation model developed by the University of Lausanne, Switzerland [14,15]. It is designed to assess the regional-scale impact of gravitational hazards, including landslides and debris flows [14,15]. The model utilizes various input data, including topography, geology, land cover, and land use, to predict areas susceptible to landslide propagation. The final output is a map showing areas potentially affected by landslides, which can be used for risk assessment in other GIS software.

3.3.2. Algorithms in Flow-R

Flow-R assesses landslide risk using two main groups of algorithms:

3.3.2.1. Algorithms for simulating landslide direction and momentum of movement

This group of algorithms includes Holmgren [22], D8 [23, 24], D∞ [25], Rho8 [26], and Freeman [27]. The Holmgren algorithm was chosen for this study due to its ability to simulate debris propagation. The Holmgren algorithm uses the equation:

$$P_i^{fd} = \frac{(\tan\tan\beta_i)^x}{\sum_{j=1}^{8}(\tan\tan\beta_i)^x} \quad (1)$$

with $\tan\tan\beta > 0$ and $x \in [1;+\infty]$

in which: i, j are the directions of material movement; Pifd is the vulnerability ratio in direction I; tanbi is the slope between the central cell and the cell in direction i; x is a parameter varying from 1 to +∞.

As “x” increases, the horizontal spread of the material flow of the landslide mass increases, and the affected area of the landslide mass widens. Claessens et al. [28] determined that when the exponent parameter “x=4”, the algorithm allows for the most suitable simulation of rock and soil landslide material propagation. To address the issue where simulations might stop when terrain changes, Holmgren [22] introduced the parameter "dh" to the algorithm, which controls changes in both terrain height and terrain slope.

When the landslide material mass moves, it generates momentum in the direction of movement. The momentum of the landslide material mass is calculated using the following formula:

$$P_i^p = \omega\alpha(i) \quad (2)$$

in which: P_i^p is the flow (movement) momentum ratio of the landslide material mass in direction i; α is the movement angle of the sliding material, based on the curvature along the inclined surface; ω is determined proportionally to the slope angle on the terrain surface, it has three implementation methods: the first is directly proportional to the surface angle of the topography, the second uses the cosine function (cosθ), and the third follows the research by Gamma [29]. For the inertial algorithm, if α=0 when 180°, it helps prevent back-propagation and saves computation time.

3.3.2.2. Algorithms for simulating the landslide impact area

The landslide impact area is calculated using a simple friction algorithm based on the energy balance equation:

$$E_{kin}^i = E_{kin}^0 + \Delta E_{pot}^i - E_f^i \quad (3)$$

in which: E^i_{kin} is the kinetic energy of the landslide material in direction i; E^0_{kin} is the initial kinetic energy of the landslide material at the initial sliding position in direction i; ΔE^i_{pot} is the change in potential energy in direction i; E^i_f is the energy loss due to friction during the movement of the landslide material in direction i. The parameter E^i_f can be calculated using two algorithms: the two-parameter friction algorithm [30] and the simple friction limit model (SFLM).

3.3.3. Input Data

The Flow-R model requires multiple spatial input layers. Input datasets included a 10 m-resolution DEM, geological and land cover maps, and a landslide inventory derived from UAV

imagery, field surveys, and Sentinel-2 data. The 10 m-resolution DEM was sourced from 1:10,000 scale topographic maps. The key parameters applied for both source area delineation and flow propagation were determined through calibration against field evidence, summarized in Table 2 and Fig. 8. The procedure for generating the landslide inventory, involving remote sensing image and Digital Elevation Model (DEM) data processing, is detailed in Fig. 9.

Table 2. Summary of Flow-R Model Input Data and Calibrated Parameters

Category	Input data/Map layer	Source/Derivation	Resolution
Input Data	DEM, Slope, Flow Accumulation, Curvature	Derived from 1:10,000 Topographic Maps	10 m
	Geology Map, Land Cover Map	Remote Sensing, Field Survey	Raster
	Landslide Inventory (33 masses)	UAV imagery, Google Earth, Field Surveys	Point/Polygon
Source Area Parameters	Slope Threshold	17 degrees	
	Flow Accumulation Threshold	0.02 ha	
	Curvature Threshold	1/100m^{-1}	
Propagation Parameters	Flow Direction Algorithm	Modified Holmgren (1994)	
	Exponent (exp)	4	
	Stop Parameter (dh)	4	
	Friction Angle	12 degrees	
	Velocity Limit	30 m/s	

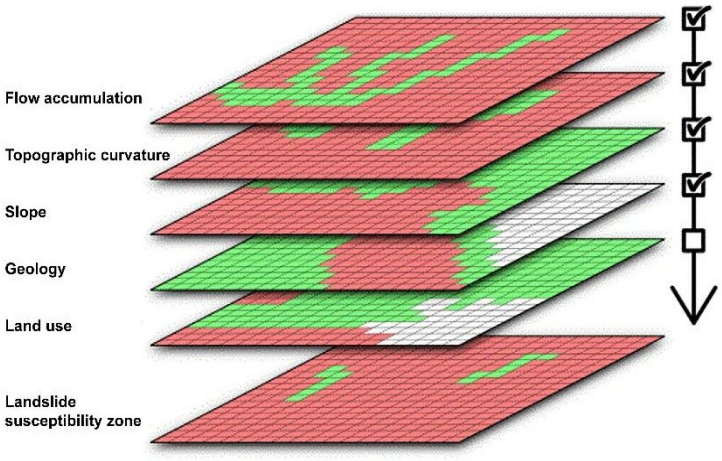

Fig. 8. Input and output data types of Flow-R models based on algorithms

3.4. Landslide inventory and source-area Identification

The landslide inventory was constructed using a combination of field surveys, UAV imagery, Sentinel-2 satellite data, and historical aerial photographs (2002–2008) (Fig 10). Potential source areas were identified through an integrated analysis of slope angle, plan and profile curvature, contributing area, and vegetation cover, and subsequently constrained using the field-verified landslide inventory to ensure that mapped initiation points correspond to real geomorphic conditions.

A total of 33 debris-flow-related landslide initiation points were confirmed in the Nam Cang sub-basin and used for calibration and validation of Flow-R. Uncertainty in the inventory remains due to dense vegetation cover, shadowing effects, and the 10-m DEM resolution, which may obscure small or shallow failures. However, targeted field verification significantly reduced misclassification and improved confidence in the mapped source areas.

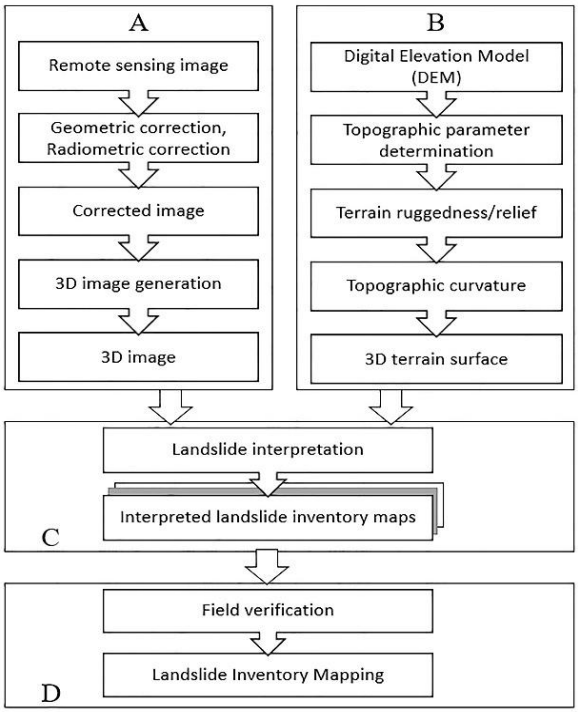

Fig. 9. Remote sensing image interpretation procedure

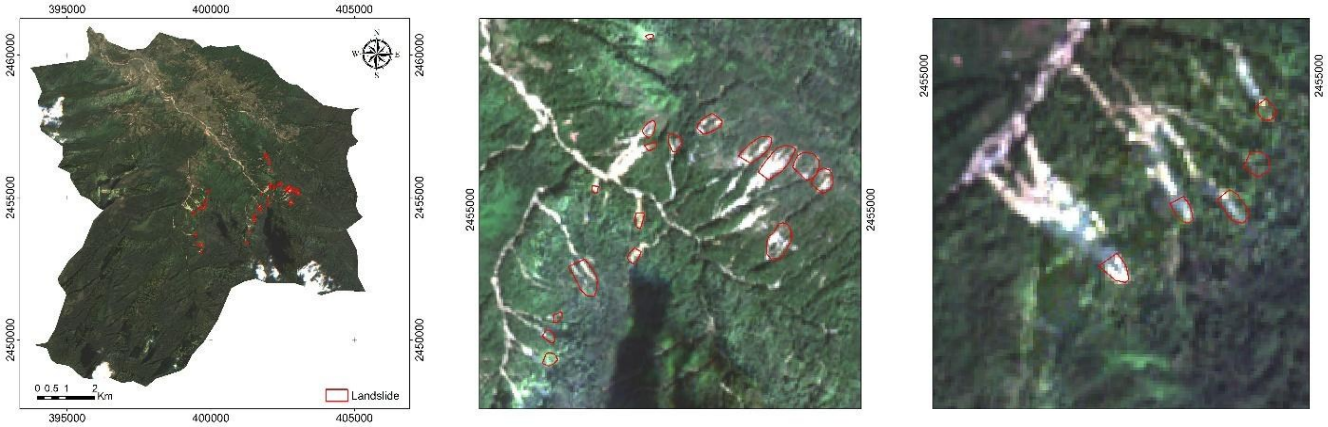

Fig. 10. Map of remotely sensed landslide identification points on Sentinel-2 imagery, cross-checked using Google Earth

3.5. Model validation and AUC assessment

Model performance was evaluated using the Receiver Operating Characteristic (ROC) curve and the Area Under the Curve (AUC) index. As commonly adopted in landslide and debris-flow susceptibility studies, validation was performed using presence-only data, and true-negative cells were not explicitly included in the AUC calculation. The obtained AUC value of 0.868 indicates that the Flow-R model has good predictive capability for debris-flow susceptibility assessment in the study area.

3.6. Model verification using the AUC index

To evaluate the predictive capability of the Flow-R model, this study uses the Area Under the Curve (AUC) index. This is a common statistical index in landslide susceptibility and disaster risk studies [31, 32].

Table 3. Assessment of FLOW-R Model Prediction Accuracy

Content	Cell on map	m²
Predicted landslide area by FLOW-R	76429	1910725
Actual landslide area determined from image	28162	704050
FLOW-R model area correctly predicted compared to actual	26465	661625

The AUC index is calculated based on the Receiver Operating Characteristic (ROC) curve. The ROC curve is built by comparing the susceptibility zoning results from the model with the actual landslide inventory map, through two measures:

True Positive Rate (TPR):

$$TPR = \frac{TP}{TP + FN} \quad (4)$$

in which (TP) is the number of landslide points or cells correctly predicted by the model, and (FN) is the number of landslide points incorrectly predicted (missed).

False Positive Rate (FPR):

$$FPR = \frac{FP}{FP + TN} \quad (5)$$

in which (FP) is the number of non-landslide points incorrectly predicted as landslides, and (TN) is the number of non-landslide points correctly predicted.

The ROC curve represents the relationship between true positive rate (TPR) and false positive rate (FPR) as the susceptibility classification threshold is varied. The AUC index is defined by the area under the ROC curve:

$$AUC = \int_0^1 TPR(FPR), d(FPR) \quad (6)$$

The AUC value ranges from 0.5 to 1.0:

* AUC = 0.5: the model has no predictive ability (random);

* 0.7 ≤ AUC < 0.8: the model has acceptable predictive ability;

* 0.8 ≤ AUC < 0.9: the model has good predictive ability;

* AUC ≥ 0.9: the model has excellent predictive ability.

In this study, the landslide and debris flow inventory map in Muong Bo Commune was used as the validation dataset to calculate the AUC index, thereby assessing the suitability of the simulation results from Flow-R. The result yielded an AUC value of 0.86, indicating that the model has good predictive ability (Table 3).

4. Results and Discussion

4.1. Geotechnical test

Fig. 11. Six soil samples for laboratory testing

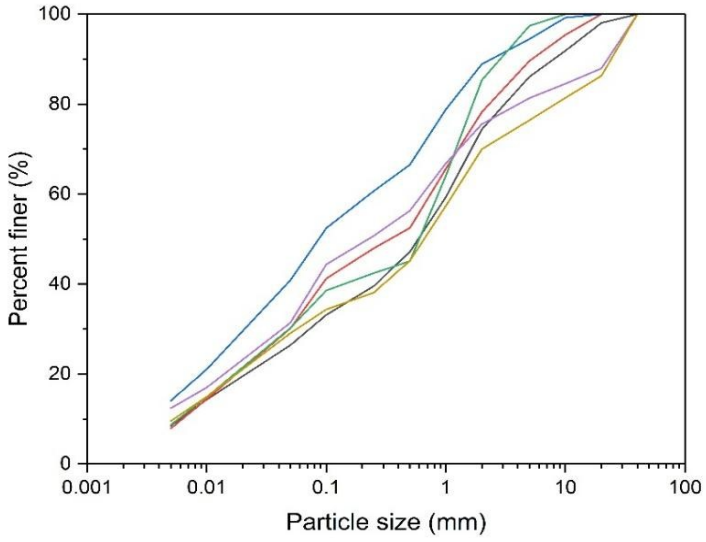

Fig. 12. Grain size distribution curves of representative soil samples

Soil samples was taken at the site a few weeks after the event, testing was conducted in the laboratory (Fig. 11). They are classified as soft to very soft Silty CLAY (CL) (Table 4), and grain size distribution analysis (Fig. 12) confirms a high fines content (~30–50% passing 0.075 mm). Crucially, the direct shear test results show that soils exhibit very low shear strength parameters (internal friction angle φ = 8°–14°; cohesion c = 6–9 kPa). Additionally, the soil has low permeability (K ~ 10-5 cm/s). The rock testing results are presented in Table 5. Rock samples show high porosity (>15%) and a significant softening coefficient (0.86–0.90). This confirms a notable reduction in rock strength

upon saturation, a key factor for instability in fractured zones.

This combination of low-strength, fine-grained soils overlying fractured, water-sensitive rock creates conditions where saturation from intense rainfall rapidly reduces shear resistance, enhancing the potential for gravitational sliding and debris flow initiation.

Table 4. Physical and mechanical properties of representative soil samples

№	Parameter	Symbol	Unit	Value						
1	Sample			C1	C2	C3	S1	S2	S3	Average
2	Moisture content	w	%	32.51	32.36	30.76	29.84	31.91	32.56	31.66
3	Specific gravity	Gs		2.67	2.67	2.69	2.69	2.69	2.68	2.68
4	Density	ρ	g/cm³	1.851	1.85	1.857	1.872	1.874	1.851	1.859
5	Dry density	ρ_d	g/cm³	1.4	1.4	1.42	1.44	1.42	1.4	1.41
6	Saturated density	ρ_{sat}	g/cm³	1.88	1.88	1.89	1.9	1.89	1.88	1.89
7	Saturation	S_r	%	95.7	95.26	92.56	92.48	96.02	95.47	94.58
8	Porosity	N	%	47.56	47.56	47.2	46.47	47.2	47.75	47.29
9	Void Ratio	e_o	-	0.907	0.907	0.894	0.868	0.894	0.914	0.90
10	Liquid limit	LL	%	35.23	35.3	34.84	32.69	34.22	35.16	34.57
11	Plasticity limit	PL	%	23.68	23.56	21.44	23.75	22.84	22.93	23.03
12	Plasticity index	PI	%	11.55	11.74	13.4	8.94	11.38	12.23	11.54
13	Liquidity index	LI	-	0.76	0.75	0.7	0.68	0.8	0.79	0.75
14	Index of compression	a_{1-2}	MPa^{-1}	0.67	0.7	0.46	0.41	0.54	0.74	0.6
15	Deformation modulus	E_{1-2}	kPa	2647	2534	5106	5650	2175	2405	3420
16	Cohesion	C	kPa	5.978	6.930	8.015	9.059	5.929	7.430	7.223
17	Angle of internal friction	ϕ	Degree	9°9'	9°31'	11°10'	13°45'	8°6'	9°26'	10.19
18	Permeability	K	cm/s	8.67E-05	7.69E-05	7.12E-05	6.24E-05	9.02E-05	8.83E-05	7.93E-05

Classification and description of soil: Silty CLAY (CL), brownish grey, yellowish brown, containing trace gravel, roots. Very soft to soft

Table 5. Physical and mechanical properties of rock samples from the study area

№	Parameter		Symbol	Unit	Value	
1	Sample				M1	M2
2	Uniaxial compressive strength	Dry		kPa	37210	34020
3		Saturated		kPa	33400	29290
4	Softening Coefficient		K_W	-	0.9	0.86
5	Natural moisture content		w	%	5.23	5.71
6	Natural density		ρ	(g/cm³)	2.468	2.458
7	Dry density		ρ_d	(g/cm³)	2.345	2.325
8	Saturated density		ρ_{sat}	(g/cm³)	2.499	2.486
9	Specific Gravity		G_S	-	2.77	2.77
10	Void ratio		e_o	-	0.181	0.191
11	Porosity		N	%	15.34	16.07

4.2. Source-area prediction and model performance

The Flow-R model correctly predicted 16 out of 33 observed debris-flow initiation points,

corresponding to a prediction rate of 48.5%. This moderate prediction rate reflects several inherent limitations of the available datasets and model structure rather than poor model performance. Specifically, Flow-R does not explicitly incorporate soil saturation, subsurface hydrological pathways, or spatially distributed rainfall intensity. Additionally, the 10-m DEM resolution is coarse relative to the scale of many small failures, and dense vegetation masks geomorphic signatures of incipient landslides The process of identifying areas prone to landslide initiation includes the following steps: (1) Data collection and synthesis, (2) Flow-R model study, (3) Study area definition, (4) Model parameter determination and component map collection, (5) Flow-R application, (6) Creation of maps of landslide initiation prone areas, and (7) Result confirmation and evaluation.

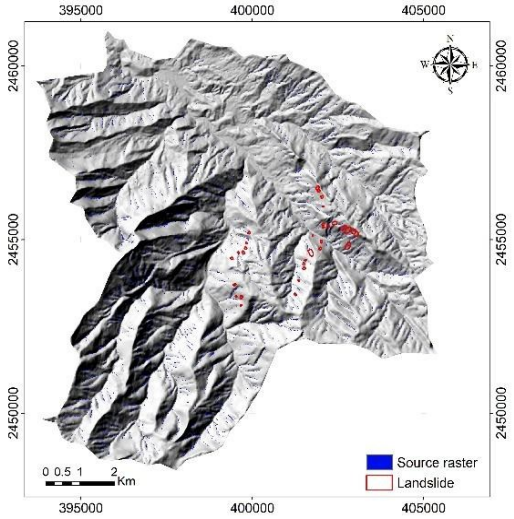

Fig. 13. Forecast diagram of predicted areas for landslide occurrence using analysis parameters derived from landslide investigation results based on remote sensing imagery

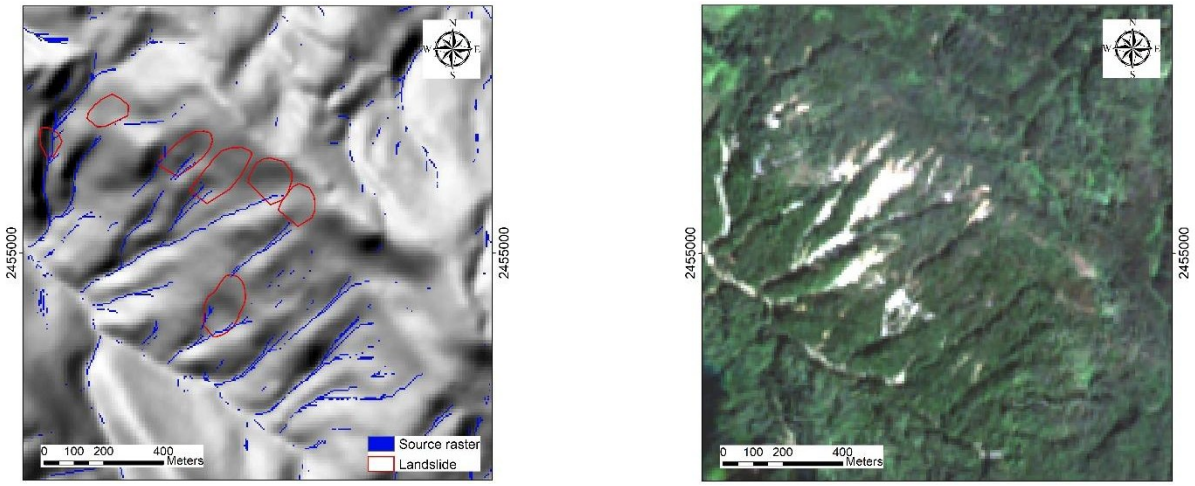

Fig. 14. Results using statistically derived parameters were verified in the field, presenting the verification results

Parameters for landslide initiation prone areas were set as follows: slope threshold 17 degrees, flow accumulation threshold 0.02 ha (200m²), curvature 1/100m⁻¹, extreme flow accumulation threshold, and vegetation cover map. The predicted map of landslide initiation risk areas, derived from analytical parameters based on remote sensing landslide inventory results, is shown in Fig. 13 and Fig. 14.

The results show that the model predicted 16 out of 33 actual landslide locations, accounting for 48.5%. This difference is attributed to factors not modeled in Flow-R, such as weathering, hydrogeology, and climate. The predicted landslide

initiation zone is considered larger than reality because it simulates the most extreme possible scenario.

4.3. Debris-flow runout assessment

Debris-Flow Runout Assessment[/RED]: The Flow-R simulations delineated plausible debris-flow propagation paths and affected zones, consistent with field observations from the September 12, 2023, event. The term “risk” is avoided here, as exposure and vulnerability components were not assessed. The results demonstrate that Flow-R is particularly effective for identifying the runout extents of medium-to-large debris flows, while smaller events tend to be overestimated due to simplified assumptions regarding friction and momentum.

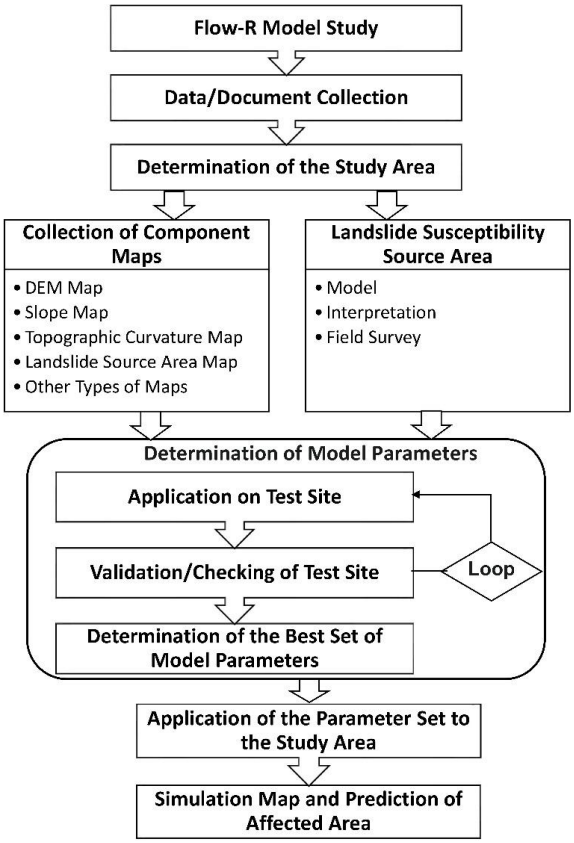

Fig. 15. Procedure for determining areas at risk of being affected by landslides

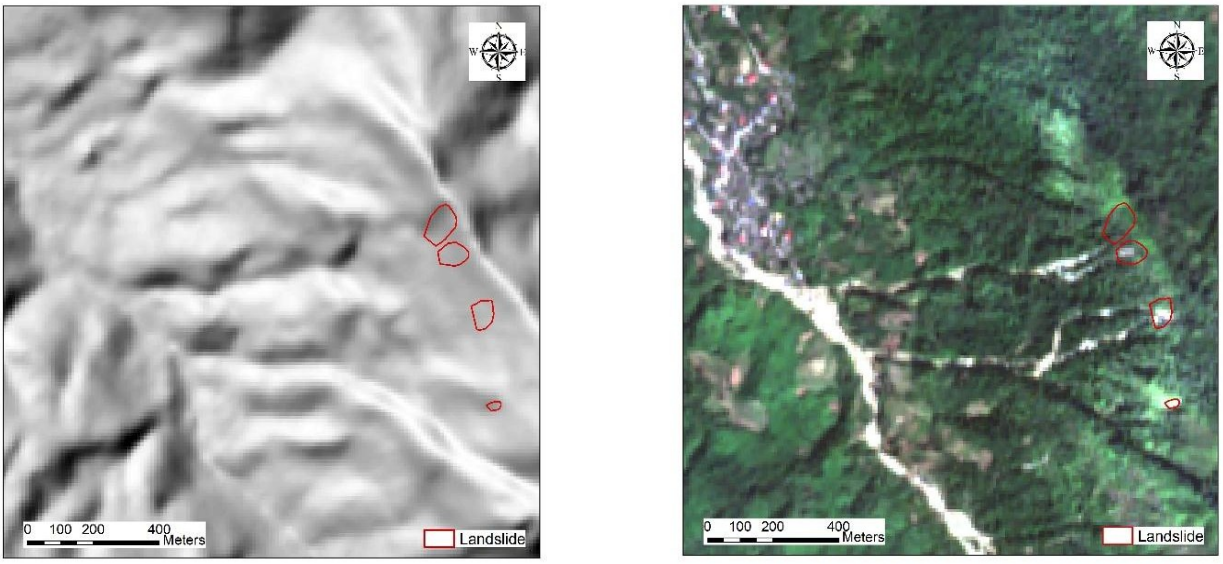

Fig. 16. Location of the verification points for test site

4.3.1. Process for identifying areas at risk of landslide impact

The process includes: data collection, Flow-R model study, research area definition, Maps of landslide initiation prone areas, model parameter determination, and creation of simulated and predicted maps of affected areas. Fig. 15. The process for identifying areas at risk of landslide impact involves the following steps. Fig. 16. The location of the verification point for test results shows the verification location.

4.3.2. Determination of model parameters and application to Nam Cang debris flow test site

A test area was selected in the Nam Cang stream area of Muong Bo Commune, based on field surveys, UAV imagery, and remote sensing data, following the debris flow event on September 12, 2023. The best results were obtained with the following parameters: Modified Holmgren (1994) with dh=4, exp=4, momentum applied proportionally to the angle, a friction angle of 12 degrees, and a velocity limit of 30 m/s. Applying this set of parameters to the verification site yielded results consistent with the actual situation observed after the debris flow. The simulation results showed good agreement with the field verification observations. Fig. 17 and Fig. 18 present the survey results and the affected area. The Nam Cang debris flow event presents a crucial real-world case for validating and refining the Flow-R model parameters under the characteristic topographic and climatic conditions of the area. The characteristics of the flood, including extreme short-duration rainfall and steep terrain, were recorded during the initial investigation.

4.3.3. Application of parameters to the study area

Following satisfactory results from the test site calibration, the optimized set of Flow-R model parameters was applied to the entire study area to simulate debris flow–affected zones. The simulation results depict the initiation and propagation areas of debris flows originating from identified source zones. The spatial distribution of debris flow susceptibility and relative probability is illustrated in Fig. 19 and Fig. 20.

Fig. 17. Survey photo at test location with code CN.914063.DK. (a)-Upper part of the landslide mass; (b)-Streambed, (c)-Transittion zone; (d)-Accumulation zone

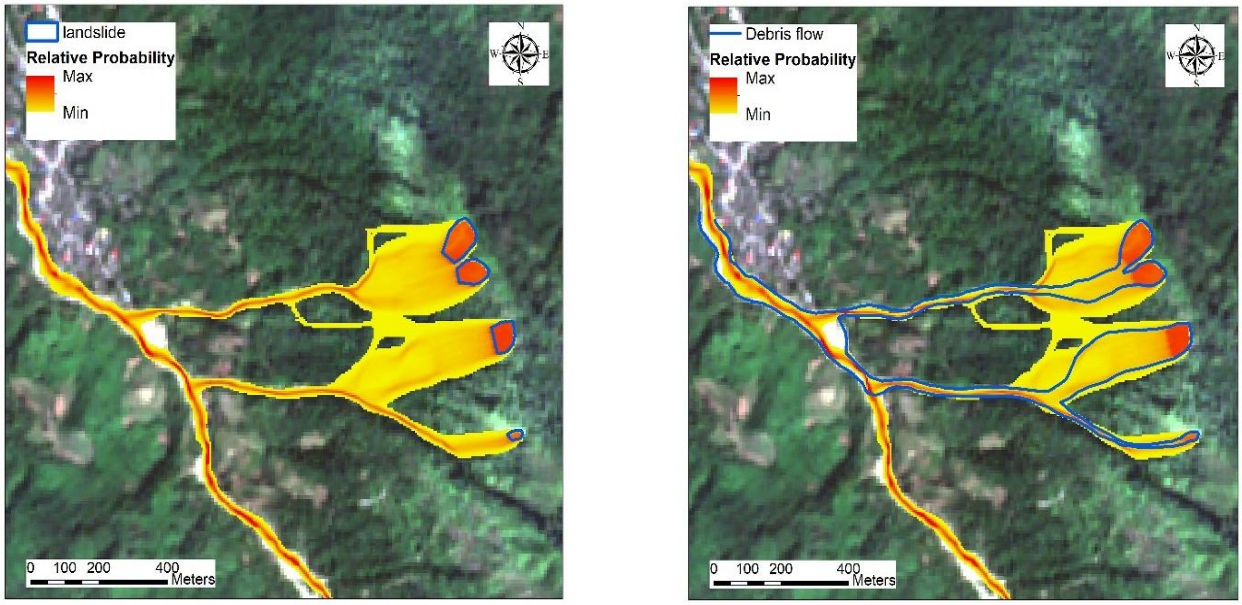

Fig. 18. The landslide-affected area at the test site. Landslide initiation zone (left image) and landslide impact zone (right image) determined by remote sensing

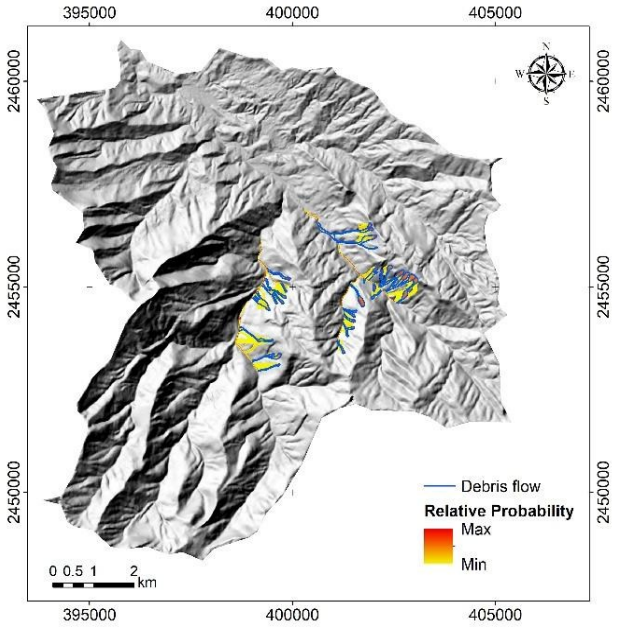

Fig. 19. Map of landslide-affected areas from the initiation zone

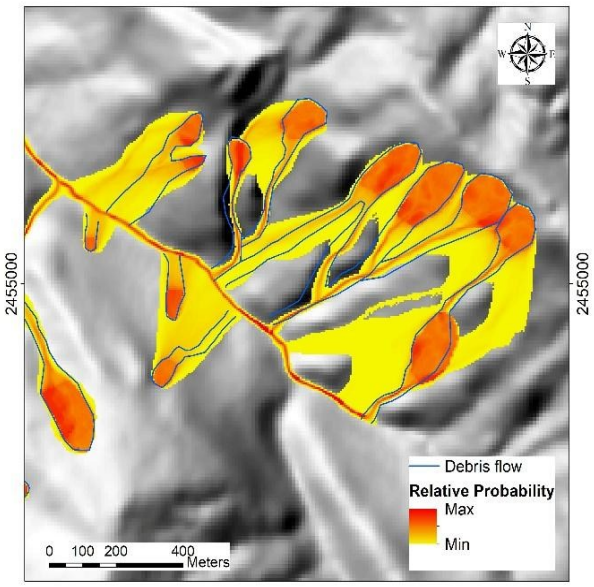

Fig. 20. Map of the landslide-affected area compared with the landslide zone determined by remote sensing imagery

The modeling results indicate that the extent of the predicted affected areas varies according to the scale of the landslide events. For more minor landslides, the model tends to overestimate the affected area, likely due to the omission of fine-scale factors such as material weathering, pore-water pressure variation, and local hydrogeological conditions. In contrast, for medium to large-scale debris flows, the simulation results exhibit a high degree of agreement with field observations and remote sensing interpretations, reflecting the model's effectiveness for large-scale hazard assessment.

The Nam Cang debris flow event, although localized, highlights the critical influence of short-duration, high-intensity rainfall and channel obstruction effects (e.g., boulder accumulation and vegetation barriers) on debris flow behavior. These

parameters warrant further refinement in future model development to improve simulation accuracy at finer spatial resolutions.

4.4. Discussion

To assess the effectiveness and reliability of the Flow-R model applied in this study, it is necessary to compare the results with those of similar studies conducted in other regions, particularly in the context of assessing geological hazard susceptibility. The Flow-R model proposed in this study employed a method to calculate the trend slope of environmental factors, such as annual rainfall and NDVI [33]. This helps to minimize errors due to time-fixed factors and improve the accuracy of geological hazard prediction models [33].

The accuracy evaluation results of the model, as measured by the AUC (Area Under the Curve) index, show that the ICM-LR model achieved 94% accuracy, and the ICM-ANN achieved 93.7% [33]. These figures significantly outperform the results of previous studies on geological hazard susceptibility assessment in Jiuzhai gully (China), where post-earthquake geological hazards frequently occur [33]. Previous studies in Jiuzhaigou reported the following AUC accuracy levels: Yi et al. achieved 81.18% with the MSS-CNN model [34], Wang et al. reached 86.89% with the DLA model [35], Yi et al. obtained 87.16% using the IWI model [36], and Cao et al. reported 85% with the ML model [37].

The improved accuracy of the Flow-R model in this study, particularly when incorporating the variation trend slope method for NDVI and annual rainfall, demonstrates its high applicability and superior potential in predicting debris flow risk and other geological hazards [33]. This provides a more reliable basis for land-use planning and disaster risk management.

5. Conclusions

This study applied and field-validated the GIS-based Flow-R model for debris-flow susceptibility and runout assessment in Muong Bo Commune, Lao Cai Province, northwestern Vietnam. Using the Nam Cang debris-flow event of 12 September 2023, the model successfully delineated debris-flow initiation and propagation zones, achieving an AUC value of 0.868, which demonstrates good predictive capability and suitability for regional-scale hazard assessment in mountainous terrain.

Geological and geomorphological analyses indicate that debris flows are primarily sourced from loose, weathered materials developed along the contact zones between the Po Sen intrusive rocks and the Ye Yen Sun metamorphic complex. Intense fracturing associated with northwest–southeast trending fault systems, combined with short-duration, high-intensity rainfall, promotes shallow landslides that frequently act as initiation points for debris flows. Field observations indicate that rainfall intensities exceeding 81.2 mm per hour, often following antecedent precipitation, play a critical triggering role.

Flow-R simulations show good agreement with observed runout zones for medium- to large-scale debris flows, while affected areas tend to be overestimated for small events. This reflects the model's simplified tr eatment of physical processes and the non-inclusion of subsurface hydrology and dynamic rainfall–runoff interactions. Nevertheless, Flow-R remains a rapid, cost-effective, and data-efficient tool for preliminary debris-flow assessment, particularly valuable in remote and data-scarce mountainous regions.

Overall, the study highlights the practical usefulness of Flow-R-derived susceptibility maps for land-use planning, infrastructure protection, and disaster risk reduction under increasing climate variability. Future improvements integrating higher-resolution topography, rainfall intensity–duration relationships, hydrological coupling, and advanced calibration approaches would further enhance model realism and predictive accuracy, supporting more robust debris-flow early warning and management strategies.

Acknowledgments

This research is funded by University of

Transport and Communications (UTC) under grant number T2025-CT-034.

References

[1]. D.V. Long, N.C. Cong, N.Q. Binh, N.T. Cuong. (2020). Assessment of the current state and research directions for landslides in Vietnam in the 2010-2020 period (in Vietnamese). *Journal of Water Resources Science and Technology*, 61, 119-128.

[2]. M. Vu. (2017). Vietnam Disaster Risk Profile. *Emergency and Disaster Reports*, 4(3), 6-61.

[3]. H.T. Tran, et al. (2025). Identification of inundated area by debris flow using LAHARZ model - A case study in the Trong La catchment in Ho Bon, Mu Cang Chai, Yen Bai. *Journal of Mining and Earth Sciences*, 66(1), 31-42. DOI: 10.46326/JMES.2025.66(1).04

[4]. T.V. Tu, D.M. Duc, N.M. Tung, V.D. Cong. (2016). Preliminary assessments of debris flow hazard in relation to geological environment changes in mountainous regions, North Vietnam. *Vietnam Journal of Earth Sciences*, 38(3), 277-286.

[5]. S.L. Gariano, F. Guzzetti. (2016). Landslides in a changing climate. *Earth-Science Reviews*, 162, 227-252. DOI: 10.1016/j.earscirev.2016.08.011

[6]. T. Le, S. Kawagoe. (2018). Impact of the landslide for a Relationship between Rainfall Condition and Land Cover in North Vietnam. *Journal of Geological Resource and Engineering*, 6, 239-250. doi: 10.17265/2328-2193/2018.06.002

[7]. D.J. Varnes. (1978). Slope movement types and processes. Special Report No. 176. Transportation Research Board Special Report, 11-33. National Academy of Sciences.

[8]. M. Jakob, O. Hungr. (2005). Debris-flow Hazards and Related Phenomena. *Springer Berlin, Heidelberg*. https://doi.org/10.1007/b138657

[9]. F. Guzzetti, A.C. Mondini, M. Cardinali, F. Fiorucci, M. Santangelo, K.-T. Chang. (2012). Landslide inventory maps: New tools for an old problem. *Earth-Science Reviews*, 112(1–2), 42-66.https://doi.org/10.1016/j.earscirev.2012.02.001

[10]. S.I. Apu, N. Sharmili, M.Y. Gazi, M.B. Mia, S.F. Sifa. (2025). Remote Sensing and GIS-Based Landslide Susceptibility Mapping in a Hilly District of Bangladesh: A Comparison of Different Geospatial Models. *Journal of the Indian Society of Remote Sensing*, 53, 531-548. DOI:10.1007/s12524-024-01988-x

[11]. R.P. Gupta. (2003). Remote Sensing Geology. *Springer Berlin, Heidelberg*. https://doi.org/10.1007/978-3-662-05283-9

[12]. S. Sorooshian, P. Nguyen, S. Sellars, D. Braithwaite, A. AghaKouchak, K. Hsu. (2014). Satellite–based remote sensing estimation of precipitation for early warning systems. Extreme Natural Hazards, Disaster Risks and Societal Implications, pp. 99-112. *Cambridge University Press*. DOI:10.1017/CBO9781139523905.011

[13]. G. Crosta, P. Frattini. (2003). Distributed modelling of shallow landslide triggered by intense rainfall. *Natural Hazards and Earth System Sciences 3*, pp. 81-93. DOI:10.5194/nhess-3-81-2003

[14]. P. Horton, M. Jaboyedoff, B. Rudaz, M. Zimmermann. (2013). Flow-R, a model for susceptibility mapping of debris flows and other gravitational hazards at a regional scale. *Natural Hazards and Earth System Sciences*, 13, 869-885, https://doi.org/10.5194/nhess-13-869-2013

[15]. P. Holmgren. (1994): Multiple flow direction algorithms for runoff modelling in grid based elevation models: An empirical evaluation. Hydrological Processes, 8(4), 327-334. doi:10.1002/hyp.3360080405

[16]. J. Blahut, P. Horton, S. Sterlacchini, M. Jaboyedoff. (2010). Debris flow hazard modelling on medium scale: Valtellina di Tirano, Italy. *Natural Hazards and Earth System Sciences*, 10, 2379-2390. https://doi.org/10.5194/nhess-10-2379-2010

[17]. R. Pastorello, T. Michelini, V. D'Agostino, (2017). On the criteria to create a susceptibility map to debris flow at a regional scale using Flow-R. Journal of Mountain Science, 14, 621-635. https://doi.org/10.1007/s11629-016-4077-1

[18]. N.T. Kiên, N.T. Hiếu, H.T. Nghĩa. (2019). A study on the ability to apply steel open-type dams against debris flow in the northern mountainous areas of Vietnam (in Vietnamese). *Journal of Science and Technology in Civil Engineering (HUCE)*, 13(5V), 28-37. https://doi.org/10.31814/stce.nuce2019-13(5V)-04

[19]. T. Xuyen et al. (2000). Geological and Mineral Resources Map of Viet Nam 1:200 000 (Bac Quang F-48-XV). *Department of Geology and Minerals of Viet Nam, Publication Permit No.212/CXB, Hanoi, 2000*.

[20]. N.D. Xuyen et al. (2000). Some seismic characteristics of the Hong River fault zone (in Vietnamese). *Vietnam Journal of Earth Sciences*, 22(4), 258-265. https://doi.org/10.15625/0866-7187/22/4/11258

[21]. N.C. Lan et al. (2023). Report of Initial investigation of Nam Cang Debris flow on 12 September 2023 in Lien Minh commune, Lao Cai.

[22]. P. Holmgren. (1994). Multiple flow direction algorithms for runoff modeling in grid base elevation models: an empirical evaluation. *Hydrological Processes*, 8(4), 327-334. https://doi.org/10.1002/hyp.3360080405

[23]. J.F. O'Callaghan, D.M. Mark. (1984). The extraction of drainage networks from digital elevation data. *Computer Vision, Graphics and Image Processing*, 28(3), 323-344.http://dx.doi.org/10.1016/S0734-189X(84)80011-0

[24]. S.K. Jenson, J.O. Domingue. (1988). Extracting Topographic Structure from Digital Elevation Data for Geographic Information-System Analysis. *Photogrammetric Engineering and Remote Sensing*, 54, 1593-1600.

[25]. D.G. Tarboton. (1997). A New Method for the Determination of Flow Directions and Upslope Areas in Grid Digital Elevation Models. *Water Resources Research*, 33(2), 309-319. https://doi.org/10.1029/96WR03137

[26]. J. Fairfield, P. Leymarie. (1991). Drainage Networks from Grid Digital Elevation Models. *Water Resources Research*, 27(5), 709-717. https://doi.org/10.1029/90WR02658

[27]. T.G. Freeman. (1991). Calculating catchment area with divergent flow based on a regular grid. *Computers & Geosciences*, 17(3), 413-422. https://doi.org/10.1016/0098-3004(91)90048-I

[28] L. Claessens, G.B.M. Heuvelink, J.M. Schoorl, A. Veldkamp. (2005). DEM resolution effects on shallow landslide hazard and soil redistribution modelling. Earth Surface Processes and Landforms, 30(4), 461-477. https://doi.org/10.1002/esp.1155

[29]. P. Gamma. (2000) DF-Walk: A debris flow simulation program for hazard zoning (in German). *Geographica Bernensia, G66, University of Bern.*

[30]. R. Perla, T.T. Cheng, D.M. McClung. (1980). A two-parameter model of snowavalanche motion. *Journal of Glaciology*, 26(94), 197-207. https://doi.org/10.3189/S002214300001073X

[31]. C.-J.F. Chung, A.G. Fabbri. (2003). Validation of Spatial Prediction Models for Landslide Hazard Mapping. *Natural Hazards*, 30, 451-472. https://doi.org/10.1023/B:NHAZ.0000007172.62651.2b

[32]. E. Yesilnacar, T. Topal. (2005). Landslide susceptibility mapping: A comparison of logistic regression and neural networks methods in a medium scale study, Hendek region (Turkey). *Engineering Geology*, 79(3–4), 251-266. https://doi.org/10.1016/j.enggeo.2005.02.002

[33]. Q. Yongping, H. Jianhua. (2025). Geological hazards susceptibility evaluaiton using ICM-

ANN and ICM-LR ensemble models (a case study of Jiuzhai gully after Mw 7.0 earthquake in 2017). *Modeling Earth Systems and Environment*, 11, 248. https://doi.org/10.1007/s40808-025-02422-y

[34]. Y. Yi, Z. Zhang, W. Zhang, H. Jia, J. Zhang. (2020). Landslide susceptibility mapping using multiscale sampling strategy and convolutional neural network: a case study in Jiuzhaigou region. *CATENA*, 195, 104851. https://doi.org/10.1016/j.catena.2020.104851

[35]. D. Wang et al. (2023). Evaluation of deep learning algorithms for landslide susceptibility mapping in an alpine-gorge area: a case study in Jiuzhaigou County. *Journal of Mountain Science*, 20, 484-500. https://doi.org/10.1007/s11629-022-7326-5

[36]. Y. Yi et al. (2019). GIS-based earthquake-triggered-landslide susceptibility mapping with an integrated weighted index model in Jiuzhaigou region of Sichuan Province, China. *Natural Hazards and Earth System Sciences*, 19(9), 1973-1988. https://doi.org/10.5194/nhess-19-1973-2019

[37]. J. Cao. (2020). Multi-geohazards susceptibility mapping based on machine learning—a case study in Jiuzhaigou, China. *Natural Hazards*, 102, 851-871. https://doi.org/10.1007/s11069-020-03927-8